Universiteit
Leiden
The Netherlands

Magnetic Patterns in CrO2 hard bars

Scheinowitz, Noa

Citation
Scheinowitz, N. (2023). *Magnetic Patterns in CrO2 hard bars*.

Version:	Not Applicable (or Unknown)
License:	License to inclusion and publication of a Bachelor or Master thesis in the Leiden University Student Repository
Downloaded from:	https://hdl.handle.net/1887/3564867

Note: To cite this publication please use the final published version (if applicable).

Magnetic Patterns in CrO_2 hard bars

THESIS

submitted in partial fulfillment of the
requirements for the degree of

BACHELOR OF SCIENCE
in
PHYSICS

Author :	Noa Scheinowitz
Student ID :	2058855
Supervisor :	Prof. Dr. J. Aarts
	Dr. K. Lahabi
Second corrector :	Dr. M.J.A. De Dood

Leiden, The Netherlands, October 2022

Magnetic Patterns in CrO_2 hard bars

Noa Scheinowitz

Huygens-Kamerlingh Onnes Laboratory, Leiden University
P.O. Box 9500, 2300 RA Leiden, The Netherlands

October 2022

Abstract

Chromium dioxide is a ferromagnet which lends itself well to applications in spintronics. Due to its strong crystalline anisotropy, it contains non-trivial magnetic states in confined structures. We investigate these magnetic patterns of CrO_2 in single crystalline nanowires, using simulations and MFM. Our simulations show that the CrO_2 nanowires with a width above 500 nm have a stripe domain magnetic pattern, while the wires with widths of and below 500 nm contain an array of vortices. Verifying this in experiments, however, has been a challenge. The MFM images show stripe domains for wires with widths of 2 μm and 1 μm. The imaging of a wire with a width of 400 nm resulted in vortex-like characteristics, although it can not be concluded for certain that these are indeed vortices.

Contents

Chapter 1

Introduction

The material discussed in this thesis is chromium dioxide (CrO_2), which is one of the very few ferromagnetic half metals. It has 100% spin polarization, which makes it promising for applications in spintronics. [1, 2] CrO_2 also has a very strong magnetocrystalline anisotropy [3], which, alongside the shape anisotropy, leads to non-trivial magnetic patterns in confined structures. In this thesis, we investigate the magnetic pattern in single crystalline nanowires.

1.1 Magnetic patterns of single-crystalline CrO_2 wires

Single-crystalline CrO_2 wires are grown epitaxially via chemical-vapor deposition. The fact that CrO_2 only grows epitaxially on TiO_2 and sapphire, makes it ideal for the selective area growth (SAG) method: one makes a trench-like mask out of SiO_x and TiO_2, where the sides and the bottom are made of SiO_x and TiO_2 respectively. Thus, when growing CrO_2 in this trench, the CrO_2 will grow in a wire form, where the width of the wire is equal to the width of the trench (see figure 1.1a for a schematic of this process). Figure 1.1b shows a scanning electron microscope (SEM) image of an L-shaped 220 nm wide wire grown using the SAG method by a group at Leiden University. [4]

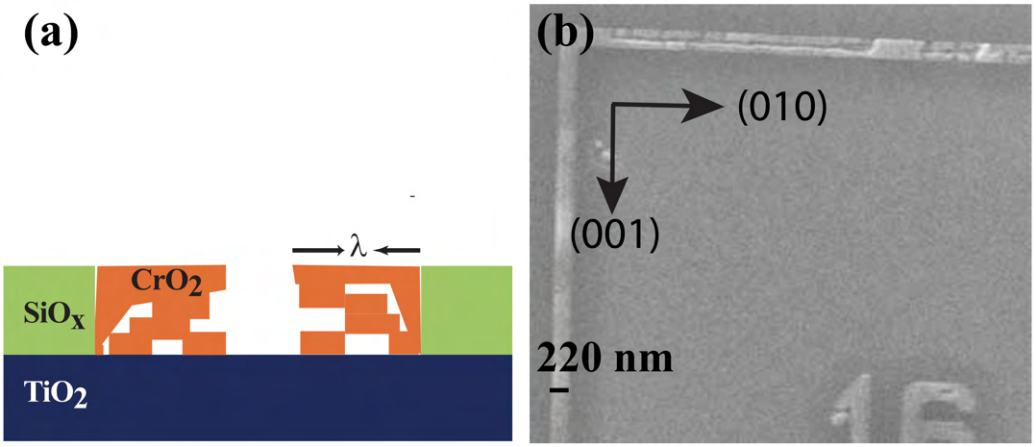

Figure 1.1: a *a schematic of the growth of a* CrO_2 *wire using SAG, where the* CrO_2 *is grown on* TiO_2 *and bounded by the* SiO_x *trench.* ***b*** *a SEM image of 220 nm wide L-shaped* CrO_2 *wire, grown for 20 min in a* SiO_x *trench. Figure taken from [4].*

Now that we know how the CrO_2 wires are grown, we must understand what causes the variety of magnetic patterns in these wires. In the absence of a magnetic field, the magnetic state of a CrO_2 wire is determined by the balance between magnetocrystalline and shape anisotropy: the magnetocrystalline anisotropy prefers the magnetisation to align with the [001] axis, while the shape anisotropy prefers it to align along the bar. This thesis focuses on hard bars, where the orientation of the bar is along the [010] axis. In that case, the magnetocrystalline anisotropy forces the magnetisation to align with the [001] axis, while the shape anisotropy forces the magnetic moments to align along the [010] axis. The relative strength of these two anisotropies gives rise to a variation of magnetic structures in the wire.

While magnetocrystalline anisotropy is an intrinsic property of the material, shape anisotropy can be tuned by varying the dimensions of system. As the width of the wire increases, the dominance of the magnetocrystalline anisotropy over the shape anisotropy increases with it. Previous simulations from Leiden University using OOMF, a software package for micromagnetic simulations, show that the competition between the two anisoptropies in a 2μm wide CrO_2 hard bar forces the magnetic pattern into a stripe domain (see figure 1.2). [5]

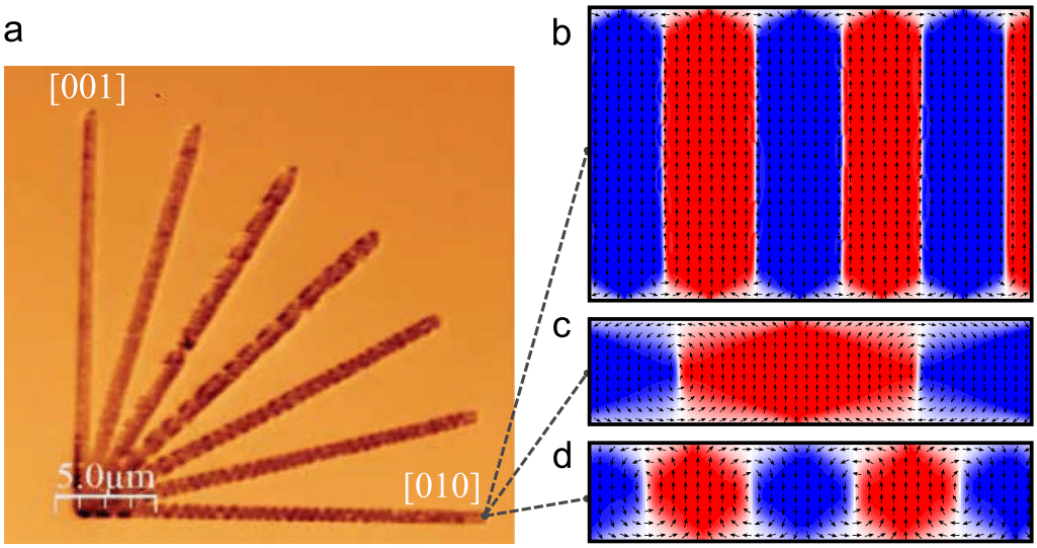

Figure 1.2: *The variety of the magnetic patterns found in a CrO_2 hard bar, depending on its width.* ***a*** *shows magnetic force microscopy imagery of CrO_2 grown along different angles respective to the [001] and [010] axis. The wire parallel to the [010] axis is the hard bar.* ***b***, ***c*** *and* ***d*** *show OOMF simulations of the magnetic patterns in 2 µm, 500 nm and 200 nm wide bars respectively. The arrows represent the in-plane magnetization. The blue and red color scheme scales with the easy axis.*

However, decreasing the width of the bar should at some point result in a state where the shape anisotropy dominates over the magnetocrystalline anisotropy so that the stripe domain becomes unstable. This raises the question if and how the magnetic structure of a narrow bar differs from a wide bar.

From figure 1.2, it becomes clear that simulations indeed suggest that reducing the width of the wire should result in a different type of magnetic structure: a vortex array. [5] A vortex is a magnetic pattern with two main properties: polarity and chirality. The center of a vortex has a strong out-of-plane magnetization, also referred to as the vortex core. The in-plane spins rotate around the vortex core in a clockwise or counterclockwise manner. A schematic representation of a vortex can be seen in Figure 1.3. A vortex array is a series of vortices next to each other (see Figure 1.4). However, in contrast to the stripe domain, this pattern has not been experimentally observed; both the concept of a vortex-like magnetic pattern in a wire and the concept of a vortex array are rare in experimental studies.

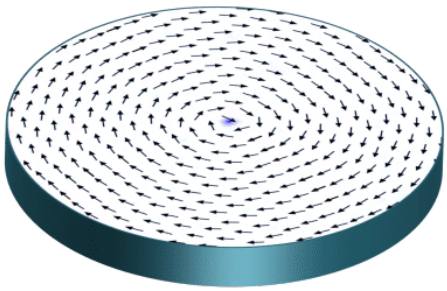

Figure 1.3: *Simulation of a magnetic vortex in a 50 nm thick Co disk. The blue dot in the center represents the vortex core, where the magnetic moments are out-of-plane. Figure taken from [5].*

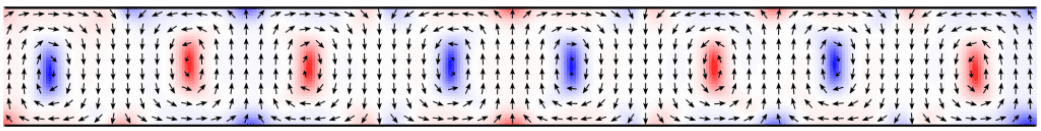

Figure 1.4: *Simulation of the magnetic pattern of a 200 nm wide* CrO_2 *hard bar, also referred to as a vortex array. The arrows represent the in-plane magnetization. The blue and red color scheme represents the out-of-plane magnetization. Figure taken from [5].*

Although past studies have imaged vortices in a variety of materials, most of them have been in dots instead of wires. [6–8] When a vortex is observed in a wire it is usually situated in a domain wall, in which case the vortex is typically metastable. [9] Reports of vortex arrays in experimental studies are rare as well. Vortex pairs are more common, f.e. a vortex pair simulated and imaged in a rectangular Permalloy thin film by applying an in-plane magnetic field sweep to the thin film. Varying the angle of the in-plane field between resulted in four different vortex pair states. [10] To our knowledge, only one paper claims to have observed an array of vortices: I. Malik et al. used variable-temperature magnetic force microscopy to image the a vortex array in 500 nm wide LSMO wires in high strain. [11]

One might ask why the concept of a vortex array is worth investigating. The answer lies in its possible application in data storage. Devices where a track of alternating up and down magnetized domain walls are used as data bits (referred to as domain wall race tracks) have been explored as contenders for low cost and fast data storage. [12] A vortex is a magnetic structure that is stable and controllable, which could make a

vortex array very capable as a data-storage device. [11]

In summary, literature shows that the magnetic pattern in CrO_2 hard bars is a stripe domain. However, although simulations predict a vortex array appears when reducing the width of the bar, this does not seem to have been proven experimentally.

In this thesis, we will attempt to find if and under what circumstances the magnetic pattern of a CrO_2 bar changes from a stripe domain to a vortex array. We will use micromagnetic simulations and magnetic force microscopy to respectively simulate and image the magnetic pattern of CrO_2 hard bars, varying both the width of the bars (ranging from 300 nm to 2 μm) and the direction of a field sweep of an external magnetic field (along and perpendicular to the easy axis). Details on both methods will be described in the theory and method chapters (chapter 2 and 3 respectively).

Version of October 2022– Created October 23, 2022 - 16:15

Chapter 2

Theory: Micromagnetic Simulations and Magnetic Force Microscopy

Before moving on to the methods we used for simulating and imaging magnetic patterns, let's focus on the theory behind both methods respectively.

2.1 Micromagnetic simulations

To calculate what magnetic state a system is in, one can use the fact that the system relaxes into the state with the lowest total energy. The total energy of the system consists of different components and can be calculated with

$$E_{tot} = \int_V (\epsilon_{ex} + \epsilon_{anis} + \epsilon_{demag} + \epsilon_z)\, dV$$

with ϵ_{ex} the exchange energy, ϵ_{anis} the anisotropy energy, ϵ_{demag} the demagnetisation energy and ϵ_z the Zeeman energy.

To determine which state corresponds to the lowest total energy, one must understand how the different components of the total energy compete with each other. The anisotropy energy prefers the magnetisation to align with the easy axis and the Zeeman energy corresponds to the external field put into the system. The exchange energy, which wants to align neighbouring spins, is the strongest interaction of the bunch, because it scales with the Curie temperature. However, its range is very short, even shorter than the exchange length. The demagnetisation energy reduces

the total magnetic moment by minimizing stray fields. Even though it is weaker than the exchange energy, it works on a much larger scale. Therefore it can compete with the exchange energy in determining which way the spins get orientated.

To calculate the effects each energy component has on the total magnetisation , one can represent the individual magnetic moments with one continuous function $\mathbf{M}(\mathbf{r})$. This is allowed when dividing the system into finite cells with dimensions smaller than the exchange length of the material: the distance over which magnetic spins interact with each other, which can vary from material to material. Therefore, when the cell size is set to a larger value than the exchange length, the results of the simulation are not physically accurate.
The total energy of each cell can then be described by

$$\epsilon_{tot} = -\int \mu_0 \mathbf{H}_{eff}(\mathbf{r}) \cdot \mathbf{M}(\mathbf{r})\, \mathrm{d}^3 r$$

$$\mathbf{H}_{eff}(\mathbf{r}) = -\frac{1}{\mu_0} \nabla \mathbf{M} \epsilon_{tot}$$

where $\mathbf{H}_{eff}$ is the continuum effective field, which consists of contributions of the external applied field, the magnetisation and the properties of the material.[13]

Now the differential of the magnetisation of each cell can be calculated using the time-dependent Landau-Lifshitz-Gilbert equation (LLG):

$$\frac{d\mathbf{M}}{dt} = \gamma \mu_0 \mathbf{M} \times \mathbf{H}_{eff} - \frac{\alpha}{M_s} \mathbf{M} \times \frac{d\mathbf{M}}{dt}$$

where M_s is the saturation magnetisation , γ is the gyromagnetic ratio and α the damping parameter.

To obtain the total magnetisation of the system, the LLG must be solved for each cell many times, so that the cells interact with each other, resolving into the lowest energy state. The results attained from micromagnetic simulations are highly accurate. [5]

2.1.1 Mumax^3

Mumax^3 is a GPU-accelerated micromagnetic simulation program, which simulates the micromagnetics of a system under a variety of chosen circumstances. [13] We used this to simulate the different groundstates the hard bars consist of, both for a field sweep in the in-plane fields. The main

principle Mumax^3 relies on is the explicit form of the Landau-Lifshitz (LL) equation:

$$\frac{\partial \mathbf{M}(\mathbf{r},t)}{\partial t} = -\frac{\gamma}{1+\alpha^2}\mathbf{M}(\mathbf{r},t)\times\mathbf{H}_{eff}(\mathbf{r},t) - \frac{\alpha\gamma}{M_s(1+\alpha^2)}\mathbf{M}(\mathbf{r},t)\times(\mathbf{M}(\mathbf{r},t)\times\mathbf{H}_{eff}(\mathbf{r},t))$$

Mumax^3 devides the geomtery into finite cuboidal cells, solving the LL eqation for each cell, which results in a system of cells where each cell has their own net magnetisation. [14]

Mumax^3 offers a variety functions to imitate the physical system. The most critical function for this research is the "Relax()" function, which resolves the system into its ground state. Mumax^3 uses the Bogacki-Shampine (RK32) method, an explicit Runge-Kutta method, to determine when the system has reached its groundstate. Mumax^3 relaxes the system by solving the LL equation for α = 1. [13] This "Relax()" function is essential, because it shows us how the most energetically favourable state changes when decreasing the width of CrO_2 hard bars.

In summary, we can simulate the magnetic states of confined structures using Mumax^3. In the method chapter (3) below, we will explain the procedure we used for simulating the magnetic texture in CrO_2 hard bars.

2.2 Magnetic Force Microscopy

Where Mumax^3 allows us to simulate magnetic patterns, Microsopic Force Microscopy (MFM) allows us to image the magnetic signals of a physical wire. This section will describe the basic principles of the imaging method.

MFM is a form of Scanning Probe Microscopy, where a probe goes over a sample to image it. By measuring the derivative of the out-of-plane magnetic stray fields from the sample, MFM results in images of the magnetism of a sample as well as its topography.

On the contrary to the closely related Atomic Force Microscopy (AFM), the tip required for MFM is magnetised and hovers above the sample. This way the magnetized tip interacts with the magnetic stray forces of the sample, because these forces are "felt" at long range (10 nm $<$ scan height $<$ 100 nm) instead of the short range Coulomb and van der Waals forces.

Imaging both the topography and the magnetic pattern of a sample at the same time is accomplished with the Hovermode, which consists of two steps. Firstly the cantilever scans the sample in TappingMode: a tapping

Version of October 2022– Created October 23, 2022 - 16:15

piezo drives the cantilever at around its resonance frequency, so that the cantilever lightly taps the sample and images the sample by scanning it line by line. It scans over a line (trace) and back over the same line (retrace), before moving on to the next scanline. This process repeats itself until the whole sample is scanned.

Because of the interaction of the magnetic cantilever with the magnetic sample, a force F_z makes the cantilever oscillate towards and from the sample, which can be described as:

$$F_z = -k\Delta z,$$

with k the spring constant of the cantilever and Δz the deflection of the cantilever. The deflection of the cantilever, in this case the distance to the sample, is measured by a position-sensitive optical deflection detector and used as the input in a feedback loop. [15] Because the surface of a sample is not completely smooth, the feedback loop adjusts the z-position of the cantilever so as to keep the deflection of the cantilever constant. By doing so, the tip-sample force F_z stays constant. Out of the change in z-position an image of the topography is made.

The second step is LiftMode: the cantilever now hovers at a higher distance (10 nm - 100 nm) and scans the same scanline (trace and retrace). Because of the increased distance between cantilever and sample, the cantilever will only pick up on the long range magnetic stray forces from the sample, meaning it can image the magnetism of the wire without topographic features showing up.

To understand how this results in magnetic images, we need to further elaborate on the movement of the cantilever. Without sample-tip interaction, the movement of the cantilever can be seen as a damped driven harmonic oscillator with resonant frequency:

$$\omega_0 = \sqrt{\frac{k}{m}}.$$

However, when there is an interaction between sample and cantilever, the force gradient $F_z' = \frac{\partial F_z}{\partial z}$ comes in to play and the spring constant changes to

$$k_eff = k - F_z'$$

The corresponding frequency shift occurs that can be described as, knowing that in MFM $F_z' \ll k$

$$\Delta\omega_0 = \omega_0' - \omega_0 \approx -\frac{F_z'}{2k}\omega_0, \Delta\omega_0 \ll \omega_0$$

Version of October 2022– Created October 23, 2022 - 16:15

and the phase shift becomes

$$\Delta\Theta = \Delta\omega_0 \frac{\partial\theta}{\partial\omega}|_{\omega_0} \approx \frac{Q}{k} F'$$

where Q is the quality factor of the cantilever.

From this phase shift, MFM translates the magnetic signal into an image of the magnetic pattern in the sample: the colors in the image from dark to light are scaled to the frequency shift from negative to positive.

In summary, MFM allows us to image the topography and magnetic pattern of a sample at the same time. In the method chapter below, we will elaborate on the parameters we used to optimize the quality of the images.

Version of October 2022– Created October 23, 2022 - 16:15

Chapter 3

Method: imaging magnetic patterns

To understand the effect of confinement on the magnetic texture of the wires, we simulated the micromagnetics of 300 nm x 7 μm x 100 nm, 500 nm x 7 μm x 100 nm and 1 μm x 7 μm x 50 nm CrO_2 hard bars using Mumax^3. Subsequently we used Magnetic force microscopy to image 2 μm, 1 μm, 500 nm and 400 nm wide CrO_2 hard bars. This chapter further elaborates on Mumax^3 and MFM respectively, first outlining the basic principles of the method and then stating the specific steps and settings we applied.

3.1 Method: Mumax^3

The parameters we used when simulating the magnetic patterns in the CrO_2 hard bars are as follows: the cell size was set to 5 nm. Because of the intrinsic properties of CrO_2 we set the saturation magnetisation M_{sat} = 4.75 $\times$ 10^5 A/m, the exchange stiffness A_{ex} = 4.6 $\times$ 10^{-12} J/m and the uniaxial anisotropy constant K_{u1} = 2,7 $\times$ 10^4 J/m^3. Because we wanted to simulate hard bars, we needed to set the uniaxial anisotropy direction to (0,1,0). The damping constant α was set to 0.5.

Mumax^3 consists of handy functions, which add certain features to the simulations. The functions we used consist of applying an external magnetic field, applying a field sweep and letting the system relax. Relaxing the system means removing the external field until the equilibrium state

is reached. Specifically, our simulations consisted of the following steps:

First we apply an external out-of-plane magnetic field (i.e. a magnetic field in the z-direction) of 2T and then let the system relax. This makes sure that the system is in its ground state before applying a field sweep.

Subsequently we apply a -500 mT in-plane external magnetic field and let the system relax. Now the bar is magnetized in one in-plane direction.

Now that the system is fully magnetized in one in-plane direction, we start the field sweep by applying an in-plane field from -150 mT to 150 mT. The field sweep consists of steps of 4 mT, each of which follow with the relaxation of the system. The jump from B_{ext} = -500 mT to B_{ext} = -150 mT and the field sweep starting there is due to the fact that the magnetocrystalline and shape anisotropy start to compete with the external magnetic field around B_{ext} = 0 T. Therefore, to be able to observe which magnetic patterns arise during this process, it is only relevant to simulate the micromagnetics in small steps from -152 mT $\leq B_{ext} \leq$ 152 mT.

We now reverse this exact process to see if there is a difference between the field sweeps in the two opposite directions: we apply a 500 mT in-plane external magnetic field and let the system relax. The bar is now magnetized in the opposite direction the simulation started of with. Subsequently the opposite in-plane field sweep is applied from B_{ext} = 152 mT to B_{ext} = -152 mT.

These steps were done for external magnetic fields in the x-direction (along the easy axis of wire) and the y direction (along the hard axis of the wire). We simulated these two field sweeps for 300 nm x 7 μm x 100 nm, 500 nm x 7 μm x 100 nm and 1 μm x 7 μm x 50 nm CrO_2 hard bars, with the halved thickness of the 1 μm wide hard bar to reduce the simulation time.

Mumax^3 computes a table with the values of different variables during each step of the simulation, by means of which the Python package used by Scheinowitz (2021) plots the in-plane and out-of-plane magnetic spins of the bars, as well as track how the total magnetisation in the field sweep-direction changes with different values of the applied field. [14] We call such a diagram an M(H) loop. These figures are presented in the section 4.1.

In summary, Mumax^3 allowed us to simulate the magnetic patterns in 1 μm, 500 nm and 300 nm wide CrO_2 hard bars, during in-plain field sweeps. The data obtained was also used to plot an M(H) loop for each of these field sweeps. The following section will describe the method we used for imaging these magnetic patterns with MFM.

3.2 MFM: Optimizing the scanning parameters

During this project, we found several scanning parameters which play a key role in the quality of magnetic images. An important aspect is the type of cantilever used, as not all cantilevers are equally qualified to image a certain sample. We tested the Bruker MESP-HM-V2 and Bruker MESP-LM-V2, the former of which lead to good results whereas the latter did not. The cantilevers have the following properties:

	MESP-HM-V2	MESP-LM-V2
Material	Si	Si
Back side coating	Reflective CoCr	Reflective CoCr
Nom. tip radius	80 nm	23 nm
Nominal coercivity	400 Oe	$<$ 400 Oe
Magnetic moment	3e-13 EMU	0.3e-13 EMU

We found that the MESP-LM-V2 resulted in images that had little contrast. This could be because of its lower nominal coercivity and magnetic moment. In addition to the cantilever choice, we found that other variables also improve the MFM imaging quality:

The scan height is the offset at which the cantilever scans the sample-line during Hovermode. Varying this offset impacts the degree to which the cantilever picks up on the magnetic stray fields of the sample. Therefore, the scan height that is too large results in a less clear magnetic image.

However, a scan height that is too small ($<$10 nm) can lead to the cantilever picking up on the van der Waals and Coulomb forces from the sample, thus imaging the topography instead of the magnetic pattern. [15] What scan height suits the best depends on the type of cantilever used and the strength of the magnetic stray fields of the sample. In the figures in MFM results section (4.2) we state which scan height we used in each measurement.

The line rate indicates the speed at which the sample is scanned. It is defined as 1/(time needed to scan the trace and retrace of one scanline). [16] By decreasing the line rate, and thus increasing the scan time, the resolution of the image increases.

We found that the scan angle defines the image quality as well. We tested two scanning directions, one where the cantilever scans the wire along the hard axis and one where the cantilever scans the wire along the easy axis. With both cantilevers used, we established that scanning along the easy axis resulted in a plain magnetic image without a magnetic pattern. A reason for this could be the type of magnetic pattern present in the

wire. The stray fields for a stripe domain as in figure 1.2 have been represented in figure 3.1. When scanning the hard axis (3.1a), the magnetic stray field continuously flips with 180 degrees, which changes F_z' and thereby images a magnetic pattern. However, when scanning along the easy axis (3.1b), the derivative of the magnetic stray field is zero. As MFM images the derivative of the magnetic stray field, no magnetic pattern will show up. In this project mostly stripe domains were imaged, which could explain the contrastless MFM images from scanning along the easy axis.

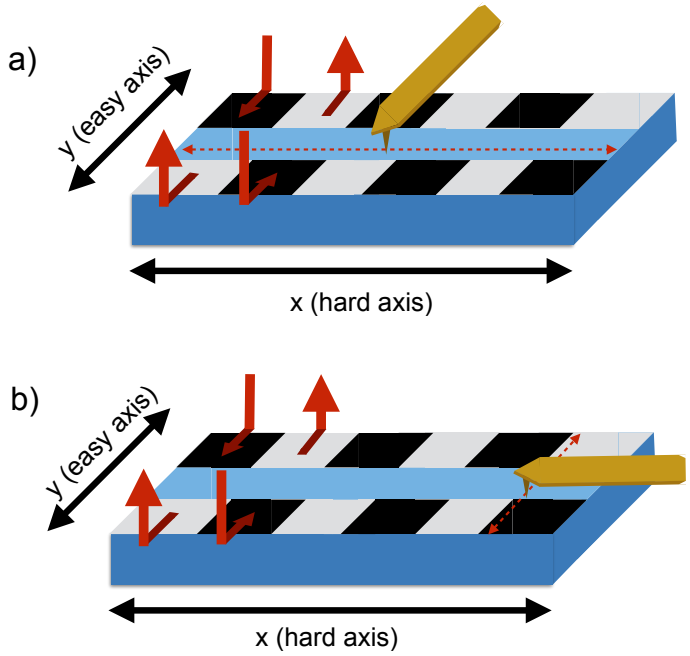

Figure 3.1: *A schematic representation of MFM on a bar with a magnetic stripe pattern. The black and grey squares represent the inward and outward pointed out-of-plain stray fields respectively (as is also represented by the red arrows).* ***a*** *the cantilever scans the sample along the hard axis (represented by the red dotted line).* ***b*** *the cantilever scans the sample along the easy axis.*

Chapter 4

Results

During this project, we used Mumax^3 to simulate the magnetisation of CrO_2 hard bars with an external magnetic field sweeping in either the y-direction or the x-direction. The simulations were done of CrO_2 hard bars with dimensions 7 μm x 1 μm x 50 nm, 7 μm x 500 nm x 100 nm and 7 μm x 300 nm x 100 nm. For all these bars, an m(H) loop and images of the magnetic pattern in the wire was produced for both the field sweep in the y-direction and the x-direction. The field sweeps were performed from -152 mT to 152 mT and back.

Subsequently, we used MFM to image CrO_2 hard bars with widths of 2 μm, 1 μm and 400 nm. Both the topography and the phase figures were obtained from these measurements.

We will present the results in the following order: firstly the Mumax^3 simulations of the 1μm, 500 nm and 300 nm wide bars respectively. From the m(H) loops it is clear that for every simulation the behaviour is mirrored for sweeps in the positive and negative sweep-direction. Therefore we will only discuss the magnetic spins from the sweep in the positive sweep-direction. This chapter also contains the magnetic pattern of a zoomed in part of the wire in this results chapter. The images of the whole wire can be found in the appendix. Subsequently we will present the results obtained from the MFM measurements of the 2 μm, 1 μm and 400 nm respectively.

4.1 Mumax^3 Results

4.1.1 1μm wide CrO_2 hard bars with a field sweep in the y-direction

This simulation is presented in figure 4.1 (m_y(H) loop and zoomed in snapshots of the bar from 0 to 3μm at certain points during the simulation) and A.1 (the whole bar at those same points during the simulation). As we increase the field in the positive y-direction, we observe from the m_y(H) loop that the number of negative spins reduces gradually. This corresponds to the snapshot 4.1.A and 4.1.B, where in B, the spins at the edges are tilted.

Increasing the field further, we observe a sudden transition in the m_y(H) loop at B_y = 16 mT (4.1.C), where now the spins in the positive y-direction should take the upper hand. From the snapshots we observe that this corresponds to a stripe domain state. We observe domain walls which are split in the middle and have a pronounced out-of-plane component. Specifically, half of the domain walls have a positive out-of-plane component and the other half are oriented negatively. There is no sign of vortices and the net magnetisation is along the positive y-direction.

Moving further along the m_y(H) loop, we observe that the number of spins in the positive y-direction gradually increase. In the snapshots this corresponds to the domains along the negative y-direction reducing in size. The domain walls pair up by getting pushed against each other, until the negative y-domains cannot get any smaller: above B_y = 32 mT (4.1.E) the negative y-domains begin to spontaneously vanish.

4.1.2 1μm wide CrO_2 hard bars with a field sweep in the x-direction

The simulation of the field sweep in the x-direction shows a very different behaviour from the field sweep in the y-direction. Specifically, from the m_x(H) loop (figure 4.2) we see that there is no hysteresis at zero field and that there is no spontaneous switching, the former meaning there is no remnant magnetisation and the latter meaning the whole process happens gradually. It is also noticeable that the field at which the bar is fully magnetised, B_x = -148 mT (4.2.A), is larger than the field at which the bar in the y-field sweep is fully magnetised.

This also becomes clear from the magnetic spins (figure A.2 and 4.2): from B_x = -64 mT upwards (4.2.B), domain walls or elongated "cores" gradually appear, with strong out-of-plane components that alternate in

up and down. Increasing the field further in the positive x-direction, the m_x(H) loop shows that the number of spins in the positive x-direction gradually take the overhand, which we can clearly see when we compare 4.2.B,C,D, and E with each other. From these snapshots, it also becomes clear that the out-of-plane components gradually weaken, until the bar is fully magnetised in the positive x-direction.

The magnetic spins (figure A.2 and 4.2) combined with the m_x(H) loop (figure 4.2) represent something that is in between stripe domains and vortices. At zero field (4.2.C) the pattern looks like a vortex array with very elongated cores. Interestingly, the domain walls or the ”cores” alternate their polarity. For normal vortices this would be highly unusual, since their polarity is randomly defined. However in this case, alternating the out-of-plane component minimises the energy associated with stray fields.

Version of October 2022– Created October 23, 2022 - 16:15

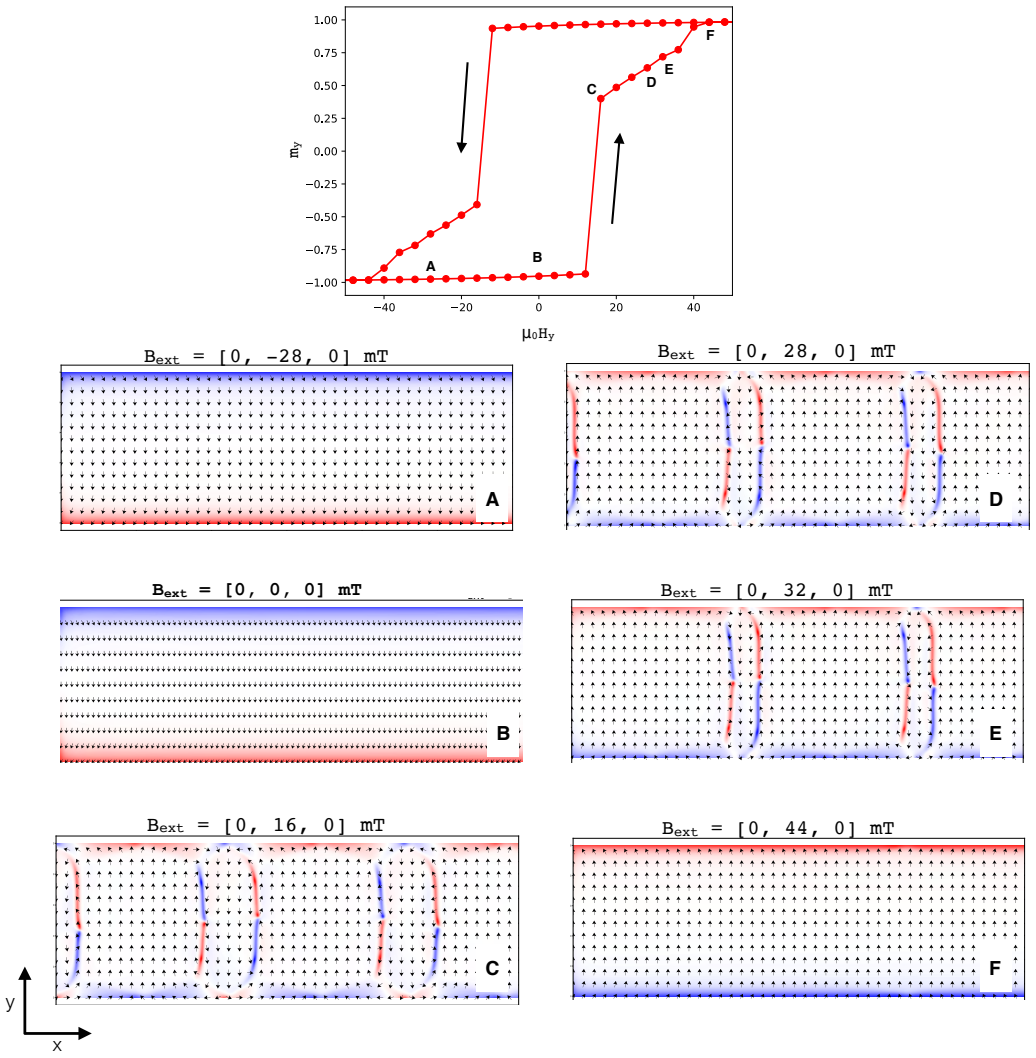

Figure 4.1: *Magnetization reversal and magnetic pattern of the 1μm wide CrO_2 bar during the field sweep in the y-direction. The horizontal axis shows magnetic fields in mT and the vertical axis shows normalised magnetisation. The images of the magnetic pattern are zoomed in to the part of the bar with the length ranging from 0 μm to 3 μm. The in-plane magnitude is represented by black vectors (a dot representing no magnitude in the x-y plane) and out-of-plane components are represented by the color scale. The total length of the wire is 7 μm and the thickness is 50 nm. It should be noted that the spin density with which snapshot B is plotted, is higher than that of snapshot A.*

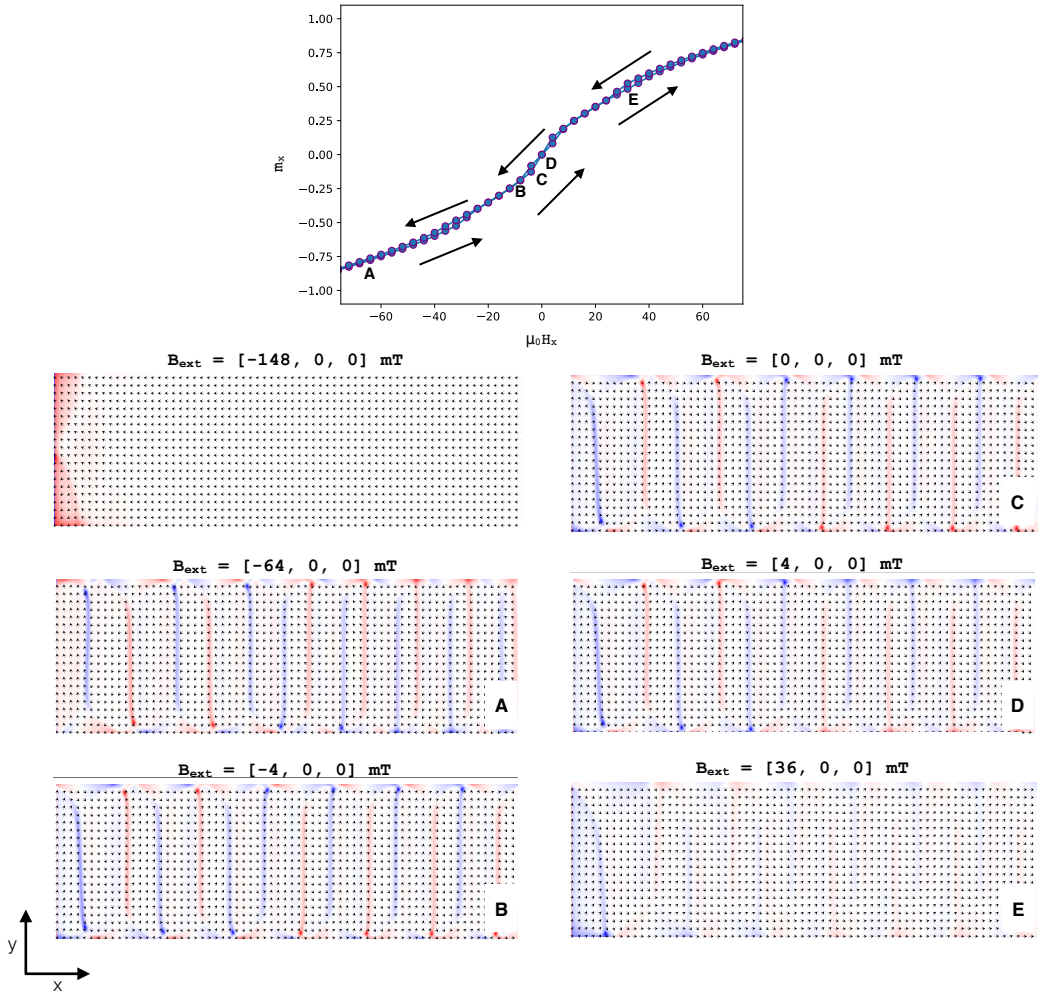

Figure 4.2: *Magnetization reversal and magnetic pattern of the 1μm wide CrO_2 bar, during the field sweep in the x-direction. The horizontal axis shows magnetic fields in mT and the vertical axis shows normalised magnetisation. The images of the magnetic pattern are zoomed in to the part of the bar with the length ranging from 0 μm to 3 μm. The in-plane magnitude is represented by black vectors (a dot representing no magnitude in the x-y plane) and out-of-plane components are represented by the color scale. The total length of the wire is 7 μm and the thickness is 50 nm.*

4.1.3 500 nm wide CrO_2 hard bars with a field sweep in the y-direction

The field sweep in the y-direction of the 500 nm wide bar shows a behaviour somewhat similar to the field sweep in the y-direction in the 1 μm wide bar. Again we see hysteresis at zero field in the m_y(H) loop, represented in figure 4.3. We observe that as we increase the field in the positive y-direction, a sudden jump appears at B_y = 6 mT. Here, the net spins in the positive y direction should be close to zero. From the magnetic spins, represented in figure A.3 and 4.3, we observe the sudden emergence of vortices at this field (4.3.D), where indeed the chirality of the vortices ensures that the number of spins in the positive and negative direction are almost equal.

Some of the vortices have regular cores and some have unconventional ”cores” that are split in two or three parts of alternating positive and negative out-of-plane components. We found the three-part vortex-like core (4.3.B and 4.3.C) in a paper where the magnetic patterns in a microsized disk where simulated for a positive to negative field sweep. [17] Depending on the diameter and thickness of the disk, the magnetic pattern can fall in a variety of different states before emerging at a vortex-state. One of these possible states is the so called buckling state. It was found that during the field sweep, a buckling state can fall into a vortex-state directly (Figure 4.4 Ia - IVa) or it can form the intermediate vortex-antivortex-vortex (VAV) triplet state (Figure 4.4 Ib - IVb). Whether or not this VAV triplet state emerges, seems to be randomly determined. [17]

It is also notable that all types of cores are tilted. It is not clear if this is an artefact of the simulation. This could be the case if the local magnetisation is trapped in an artificial knot. Unfortunately, determining whether these ”cores” are physical with MFM would be very challenging, as the resolution and the out-of-plane stray fields would have to be big enough to clearly observe these ”cores”.

At B_y = 66 mT (4.3.E), we observe that the domains of some of the vortices spontaneously disappear. At B_y= 74 mT (4.3.F) the bar is fully magnetised in the positive y-direction.

4.1.4 500 nm wide CrO_2 hard bars with a field sweep in the x-direction

The m_x(H) loop of the field sweep in the x-direction of the 500 nm wide bar ((Figure 4.5) shows hysteresis on the sides, but not in the middle.

The magnetic spins (see figures A.4 and 4.5) show a magnetic pattern that resembles vortices a lot. Starting at B_x = -44 mT (4.5.B), more and more vortex cores gradually appear. At B_x = -36 mT (4.5.D) we observe an array of vortices with a random distribution of positive and negative vortex cores. The vortex cores seem to be stretched out, which may again be an artefact of the simulation. From B_x = 36 mT (4.5.F) upwards, the vortex cores get pushed towards the sides of the bars, ultimately resulting in the vortices disappearing from the bar and the bar being fully magnetised in the positive x-direction.

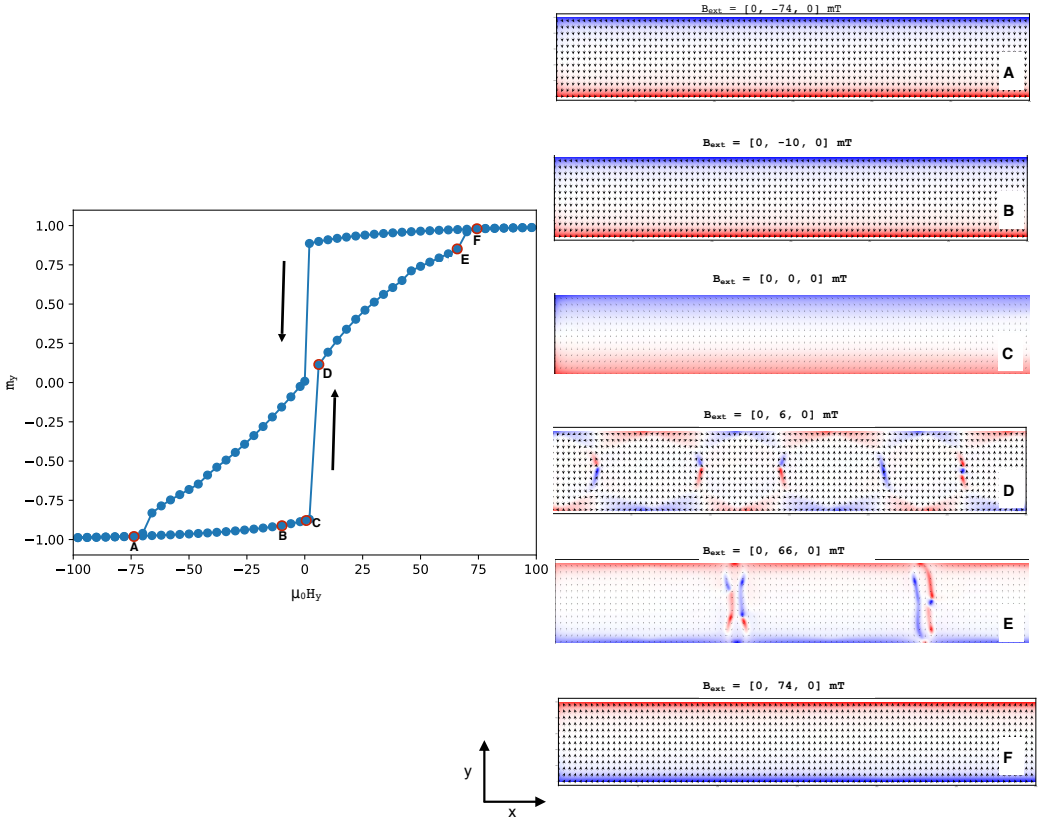

Figure 4.3: *Magnetization reversal and magnetic pattern of the 500 nm wide* CrO_2 *hard bar during the field sweep in the y-direction. The horizontal axis shows magnetic fields in mT and the vertical axis shows normalised magnetisation. The images of the magnetic pattern are zoomed in to the part of the bar with the length ranging from 0 µm to 3 µm, during the field sweep in the y-direction. The in-plane magnitude is represented by black vectors (a dot representing no magnitude in the x-y plane) and out-of-plane components are represented by the color scale. The total length of the wire is 7 µm and the thickness is 100 nm.*

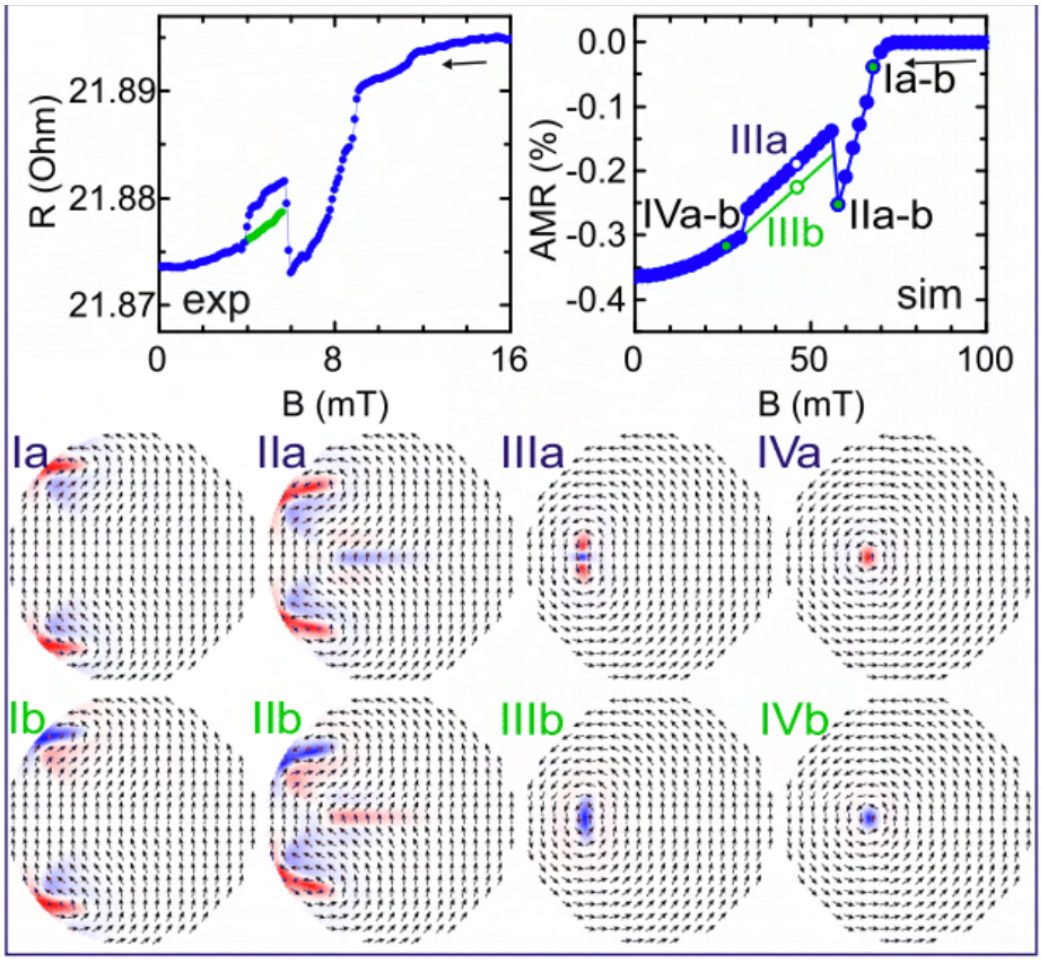

Figure 4.4: *AMR data and simulations of a disk with diameter = 4 μm and thickness = 50 nm. Both Ia - IVa and Ib - IVb show the formation of a vortex-state from a buckling state. In Ia - Iva an intermediate the process goes through an intermediate VAV triplet state, whereas in Ib - IVb the vortex-state is formed directly. Figure taken from [17].*

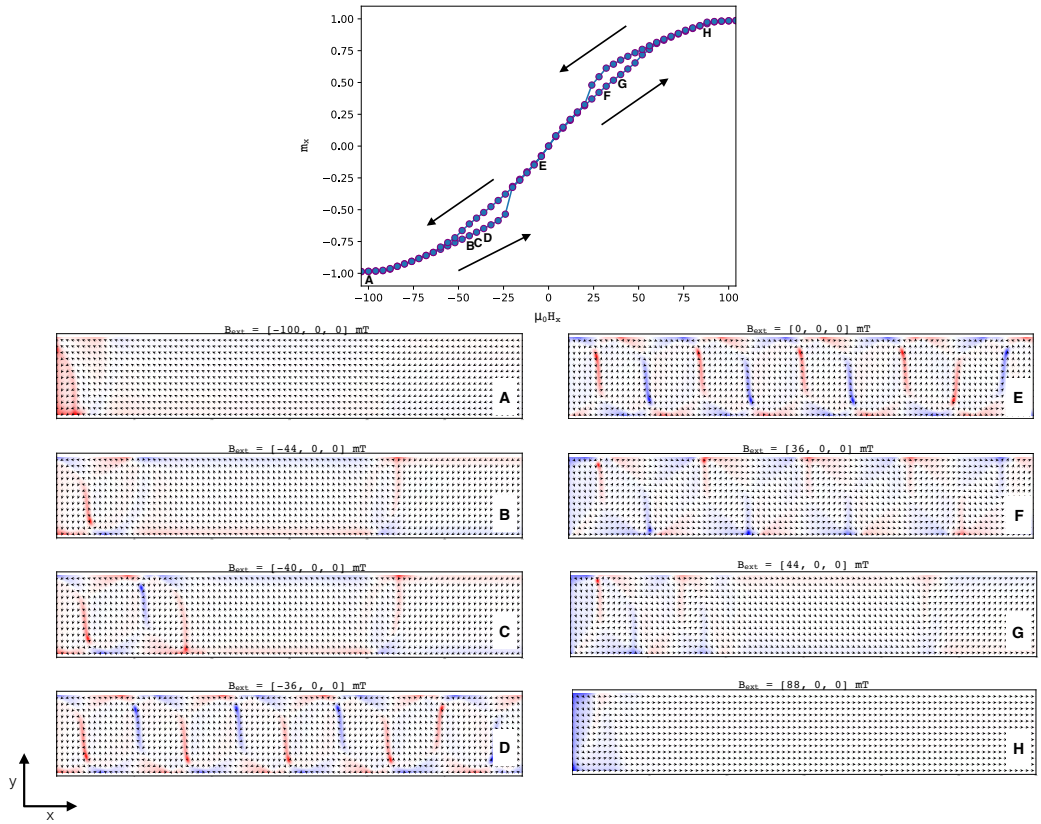

Figure 4.5: *Magnetization reversal and magnetic pattern of the 500 nm wide* CrO_2 *bar, during the field sweep in the x-direction. The horizontal axis shows magnetic fields in mT and the vertical axis shows normalised magnetisation. The images of the magnetic pattern are zoomed in to the part of the bar with the length ranging from 0 µm to 3 µm. The in-plane magnitude is represented by black vectors (a dot representing no magnitude in the x-y plane) and out-of-plane components are represented by the color scale. The total length of the wire is 7 µm and the thickness is 100 nm.*

4.1.5 300 nm wide CrO_2 hard bars with a field sweep in the y-direction

From all the bars simulated, the field sweep in the y-direction of the 300 nm wide bar shows the most clear vortex array. The m_y(H) loop (figure 4.6) shows no hysteresis in the middle, but does show it on the sides.

We observe in the m_y(H) loop that at B_y = -18 mT a sudden jump occurs, where the number of spins in the negative y-direction reduces considerably. From the magnetic spins (figures 4.6 and A.5) we see that this jump corresponds to a vortex array spontaneously occuring (4.6.B). Similar to the field sweep in the y-direction in the 500 nm wide bar, the vortex cores are tilted and we observe the VAV triplet state. The distribution of positive and negative vortex cores is random.

Increasing the field further increases the number of spins in the positive y-direction (4.6.C,D), until at B_y = 82 mT (4.6.E) some of the cores spontaneously disappear from the bar. From B_y = 90 mT (4.6.F), the bar is fully magnetised in the positive y-direction.

4.1.6 300 nm wide CrO_2 hard bars with a field sweep in the x-direction

The m_x(H) loop (see figure 4.7) shows hysteresis in the middle. We observe that increasing the field in the positive x-direction, results in the gradual increase of spins in the positive x-direction, until at B_x = 8 mT a sudden increase in these spins appears. However, from the snapshots during the simulation (figures 4.7 and A.6) we observe that at B_x = 0 mT (4.7.C), the spins in the positive x-direction take the overhand, contrary to the m_x(H) loop. We suspect that there is an offset in the data which causes this mismatch.

However, we can still observe the general the magnetisation process qualitatively from the snapshots. We observe that increasing the field in the positive x-direction results in the magnetisation of the bar in the negative y-direction. We also observe that the positive out-of-plane component gradually increases. Increasing the field further gradually magnetises the bar in the positive x direction.

We also observe from the spin snapshots (A.6 and 4.7) that a dot with a negative out-of-plane component starts to appear (4.7.A), moving almost exactly to the middle of the bar (4.7.B). When increasing the field in the positive x-direction, the spot starts moving up. In 4.7.C we can see clearly that the in plane field components are gyrating around it in counter clock-

Version of October 2022– Created October 23, 2022 - 16:15

wise. Increasing the field further in the positive x-direction, the vortex moves to the upper edge of the bar and disappears in 4.7.D. Although this phenomenon ticks off the two specifics of a vortex, a vortex core and a chirality, we are not convinced that it is physical. The fact that the "core" appeared in the middle of the bar only, makes it likely that this is an artefact of the simulation.

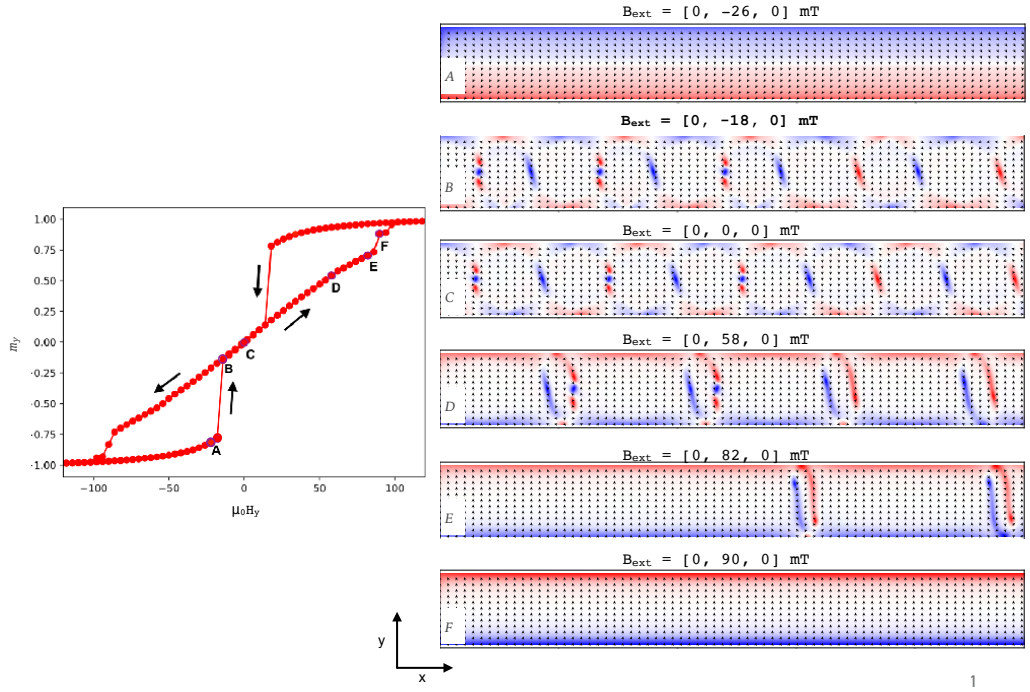

Figure 4.6: *Magnetization reversal and magnetic pattern of the 300 nm wide* CrO_2 *bar during the field sweep in the y-direction. The horizontal axis shows magnetic fields in mT and the vertical axis shows normalised magnetisation. The images of the magnetic pattern are zoomed in to the part of the bar with the length ranging from 0 μm to 2,5 μm. The in-plane magnitude is represented by black vectors (a dot representing no magnitude in the x-y plane) and out-of-plane components are represented by the color scale. The total length of the wire is 7 μm and the thickness is 100 nm.*

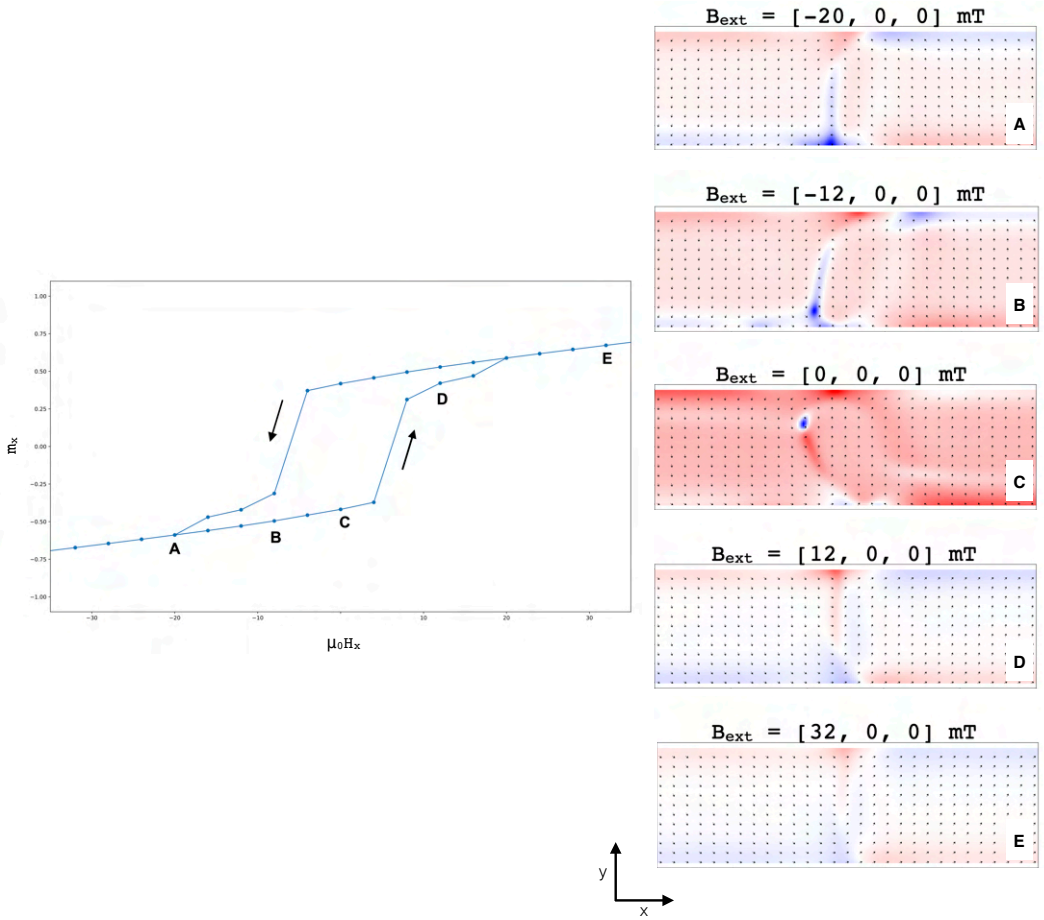

Figure 4.7: *Magnetization reversal and magnetic pattern of the middle part of the 300 nm wide CrO_2 bar during the field sweep in the x-direction. The horizontal axis shows magnetic fields in mT and the vertical axis shows normalised magnetisation. The images of the magnetic pattern have been zoomed in to the middle of the bar ($\leq$ 3μm$\leq$ 4μm), because there the magnetisation is atypical. The in-plane magnitude is represented by black vectors (a dot representing no magnitude in the x-y plane) and out-of-plane components are represented by the color scale. The total length of the wire is 7 μm and the thickness is 100 nm.*

4.2 Magnetic Force Microscopy Results

This section presents the MFM images we made of CrO_2 hard bars with widths of 2 μm, 1 μm and 400 nm respectively. In order to determine if an element in the magnetic pattern is caused by topographic crossover, both the topography and phase image are shown for each result.

From the Mumax^3 results, presented in section 4.1, we expect to see stripe patterns for 2 μm and 1 μm wide bars and a vortex array for the 400 nm wide bar. The difficulty in imaging these patterns with MFM is the similarity between the two: when comparing the simulations of the stripe pattern (4.1.C) and the vortex array (4.6.C), we see that both have alternating out-of-plane fields on the edges of the bar. The distinguishing factor is that the stripe pattern shows stripes consisting half of positive and half of negative out-of-plane fields connecting the two edges of the bar, whereas the vortex array shows a vortex cores along the middle of the bar. The MFM results below will indeed show these elements distinguishing the stripe patterns from the vortex arrays.

4.2.1 2 μm wide CrO_2 hard bar

Figures 4.8a.1 and 4.8b.1 show the topography of the 2 μm wide hard bar, with figure 4.8b.1 being a zoomed in image of figure 4.8a.1. The surface of the bar is relatively smooth, varying in height in the order of 10 nm. Therefore, the topography does not influence the magnetic images to the degree that they do not represent the stray magnetic fields from the bar, although we do see some topographic crossover in the light spots present in both the topography and the phase figures.

The phase figures, 4.8a.2 and 4.8b.2, present a relatively regular pattern on the edge of the wire of dark spots opposite to lights spots, which matches the pattern one would expect for a stripe domain. In between the edges, there are light stripes opposite to dark stripes, which matches the out-of-plane stray fields in the Mumax^3 results (4.1.C).

4.2.2 1 μm wide CrO_2 hard bar

Figure 4.9a.1 shows the topography of a 1 μm wide CrO_2 hard bar. Figure 4.9b.1 shows the topography of a zoomed in part of the same bar. Comparable to the 2μm MFM images, we observe a pattern of dark spots opposite light spots. However, the spots seem to be tilted. It is also noticeable that the topographic features are not translated to the phase figures. This is

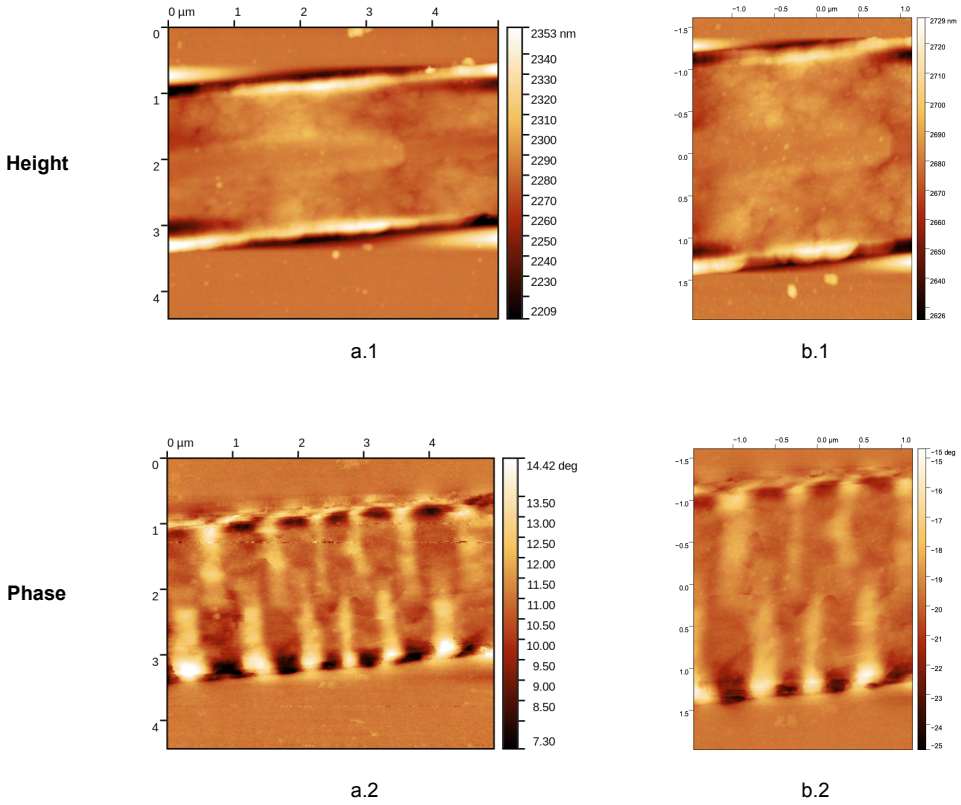

Figure 4.8: *MFM imaged topography and phase of the 2 μm wide CrO_2 bar (a.1 and a.2) and a zoomed in part of the same bar (b.1 and b.2). Scan height = 30 nm. For the overview (a.1 and a.2) the Line rate = 0.5 Hz. For the zoomed in images (b.1 and b.2) the Line rate = 0.2 Hz. Cantilever: Bruker MESP-HM-V2.*

surprising, as the scan height is as high (30 nm) as it is in the 2 μm images (figure 4.8), where the topography did show up in the phase figures.

4.2.3 400 nm wide CrO_2 hard bar

When trying to image a 400 nm wide CrO_2 hard bar, it is good to know that finding a presteen and non broken crystal is challenging, resulting in most crystals being broken in sections. We imaged multiple 400 nm wide bars and imaged multiple places in those bars. The images shown here (figures 4.10, 4.11 and 4.12) are all images of different parts of the same bar. Although these parts of the bar are broken into segments, they contain parts of relatively homogeneous height ($<$ 100 nm), which was challenging to find.

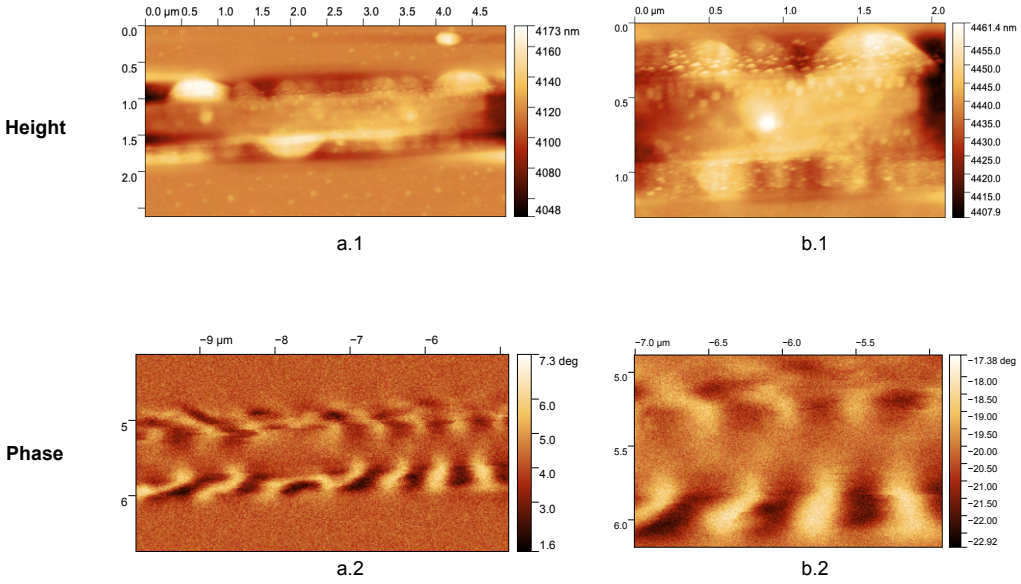

Figure 4.9: *MFM imaged topography and phase of the 1 μm wide* CrO_2 *bar (a.1 and a.2) and a zoomed in part of the same bar (b.1 and b.2). Scan height = 30 nm, Line rate = 0.5 Hz. Cantilever: Bruker MESP-HM-V2.*

In figure 4.10, we observe light spots opposite dark spots on the edges of the bar, which we expect from the Mumax^3 results. We also see two light spots that are present in both the topography and the phase image. These spots are encircled in pink. However, a closer examination reveals a dark spot that is only present in the phase image (encircled in blue). The spot exists in the centre of a quartet of dark and light spots on the edges of the bar, which corresponds exactly to the Mumax^3 results (4.6.C). This could mean that that dot imaged is a vortex core. The fact that the dot is not visible in the rest of the bar, could be because the bar is broken into segments, so that only in a small part where the the height is homogeneous, a vortex is visible.

Similarly, in figure 4.11, the topography and phase images of a different part of the same 400 nm wide bar, we observe a series of alternating dark and light spots on the edges of the bar, as expected from both a stripe pattern and a vortex array. More interestingly however, are the dots that only appear in the phase figures (encircled in blue) and thus are not topographic features. Again they exist in a small segment of the wire with homogeneous height and are positioned in the centre of a quartet of negative and positive out-of-plane fields on the edges. This once more corresponds to the vortex array in the Mumax^3 results of the field sweep in the

y-direction in the 300 nm wide bar (4.6.C).

Figure 4.12 shows the topography and phase image of yet again a different part of the same 400 nm wide bar. As we can see encircled in pink, some topographic features are crossed over to the phase image. However, a dark spot (encircled in blue) is only visible in the phase image. This again could be the magnetic signal of a vortex core.

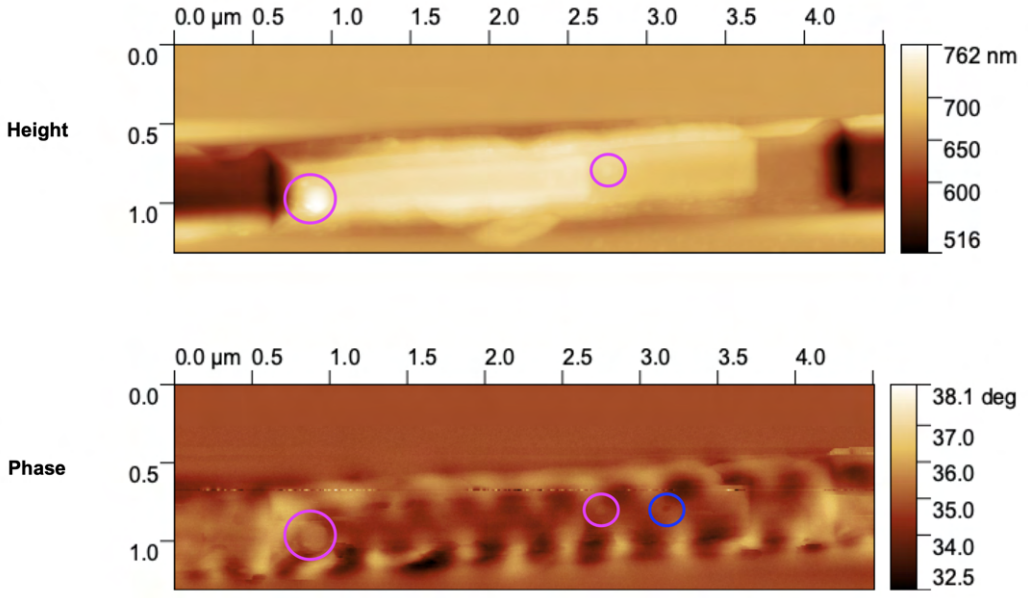

Figure 4.10: *MFM imaged topography and phase of a 400 nm wide* CrO_2 *bar. Scan height = 30 nm, Line rate = 0.1 Hz. Cantilever: Bruker MESP-HM-V2. The spot only visible in the phase figure is encircled in blue. Topographic features present in the phase image are encircled in pink. The disruptive line seen in the the phase figure is most likely due to the tip hitting the sample during the measurement.*

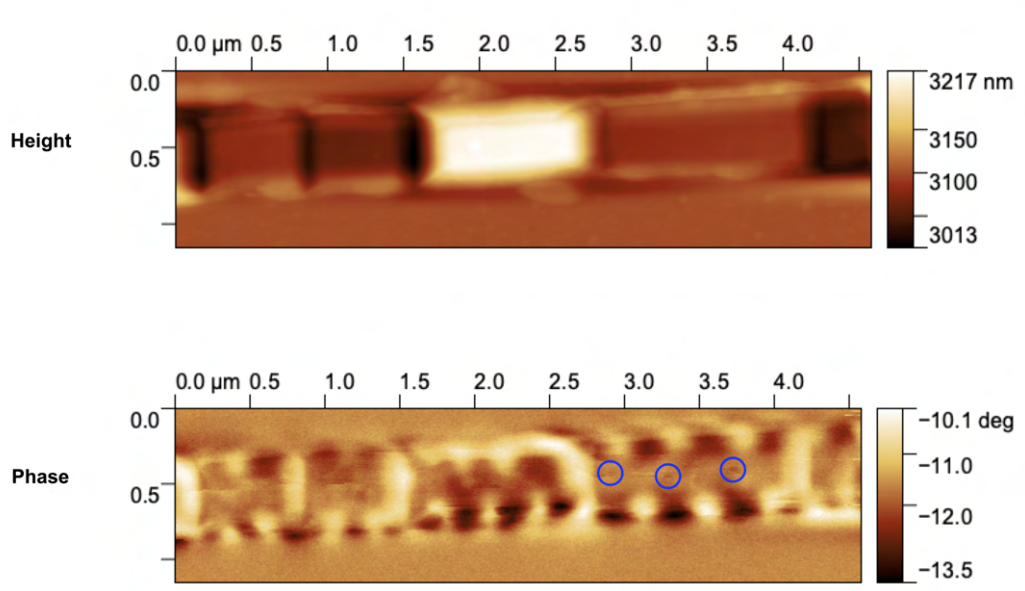

Figure 4.11: *MFM imaged topography and phase of a 400 nm wide* CrO_2 *bar. Scan height = 30 nm, Line rate = 0.5 Hz. Cantilever: Bruker MESP-HM-V2. Dark spots which are only visible in the phase figure, possibly vortex cores, are encircled in blue.*

Version of October 2022– Created October 23, 2022 - 16:15

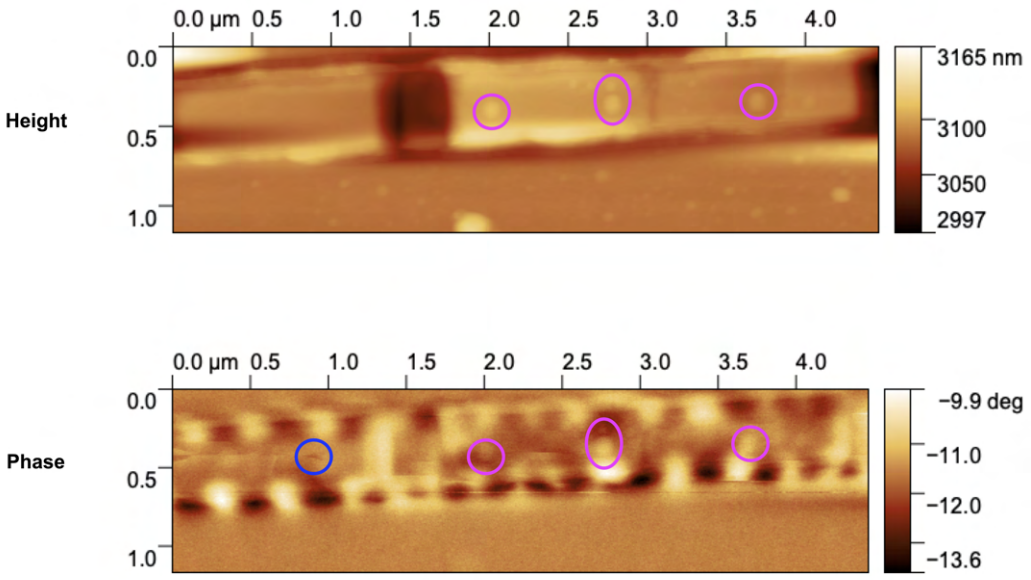

Figure 4.12: *MFM imaged topography and phase of a 400 nm wide* CrO_2 *bar. Scan height = 30 nm, Line rate = 0.5 Hz. Cantilever: Bruker MESP-HM-V2. A dark spot which is only visible in the phase figure, possibly a vortex core,is encircled in blue. The light spots showing up in both the topography and phase figure are encircled in pink.*

Chapter 5

Conclusion

This thesis consists of a comparison of Mumax^3 simulations and MFM measurements on the magnetic patterns CrO_2 hard bars. We used Mumax^3 to simulate the field sweeps in the x-direction and y-direction of 7 μm x 1 μm x 50 nm, 7 μm x 500 nm x 100 nm and 7 μm x 300 nm x 100 nm CrO_2 hard bars. From each simulation we obtained the corresponding M(H) loop and plots of the magnetic pattern of the bars.

We then imaged CrO_2 hard bars with widths of 2μm, 1μm and 400 nm, resulting in images of the topography and phase.

From the Mumax^3 results, we can conclude that vortices become more favourable as the width of the wires reduces. We observed vortex arrays in the 500 nm wide and 300 nm wide wires, when a field sweep in the y-direction was performed. The MFM results indicate that the results from the simulations might be physical, as some signatures of vortex cores in the 400 nm wide CrO_2 hard bars were observed. However, the vortex states depend on how the sample is prepared. Therefore we need more data on homogeneously grown 400 nm wide wires to be certain of this phenomenon.

In conclusion, the phenomenon of a vortex array in CrO_2 hard bars seems plausible, although more research on the matter should be done to conclude this for certain.

Bibliography

[1] X. Zou and G. Xiao, *Electronic transport and magnetoresistance in polycrystalline and epitaxial CrO2 nanowires*, Physical Review B **77** (2008), Publisher: American Physical Society.

[2] C. König, M. Fonin, M. Laufenberg, A. Biehler, W. Bührer, M. Kläui, U. Rüdiger, and G. Güntherodt, *Micromagnetism and magnetotransport properties of micron-sized epitaxial CrO2 wires*, Physical Review B **75**, 144428 (2007), Publisher: American Physical Society.

[3] I. Heukensfeldt Jansen, *Engineering Magnetic Domain Walls in Magnetic Nanowires*, Master's thesis, Leiden University.

[4] A. Singh, C. Jansen, K. Lahabi, and J. Aarts, *High-quality CrO 2 nanowires for dissipation-less spintronics*, Physical Review X **6**, 041012 (2016).

[5] K. Lahabi, *Spin-triplet supercurrents of odd and even parity in nanostructured devices*, PhD thesis, 2018, ISBN: 9789085933755, OCLC: 1083103736.

[6] T. Shinjo, T. Okuno, R. Hassdorf, â. K. Shigeto, and T. Ono, *Magnetic Vortex Core Observation in Circular Dots of Permalloy*, Science **289** (2000), Publisher: American Association for the Advancement of Science.

[7] K. Y. Guslienko, X. F. Han, D. J. Keavney, R. Divan, and S. D. Bader, *Magnetic Vortex Core Dynamics in a Ferromagnetic Dot*, Physical Review Letters **96** (2006), arXiv: cond-mat/0510595.

[8] T. Okuno, K. Shigeto, T. Ono, K. Mibu, and T. Shinjo, *MFM study of magnetic vortex cores in circular permalloy dots: behavior in external field*, Journal of Magnetism and Magnetic Materials **240**, 1 (2002).

[9] R. Moriya, L. Thomas, M. Hayashi, Y. B. Bazaliy, C. Rettner, and S. S. Parkin, *Probing vortex-core dynamics using current-induced resonant excitation of a trapped domain wall*, Nature physics **4**, 368 (2008).

[10] J. Li, Y. Wang, J. Cao, X. Meng, F. Zhu, and R. Tai, *The control of magnetic vortex state in rectangular nanomagnet*, Journal of Magnetism and Magnetic Materials **451**, 379 (2018).

[11] I. A. Malik, H. Huang, Y. Wang, X. Wang, C. Xiao, Y. Sun, R. Ullah, Y. Zhang, J. Wang, M. A. Malik, I. Ahmed, C. Xiong, S. Finizio, M. Kläui, P. Gao, J. Wang, and J. Zhang, *Inhomogeneous-strain-induced magnetic vortex cluster in one-dimensional manganite wire*, Science Bulletin **65**, 201 (2020).

[12] S. S. Parkin, M. Hayashi, and L. Thomas, *Magnetic domain-wall racetrack memory*, Science **320**, 190 (2008).

[13] A. Vansteenkiste, J. Leliaert, M. Dvornik, M. Helsen, F. Garcia-Sanchez, and B. Van Waeyenberge, *The design and verification of MuMax3*, AIP Advances **4** (2014).

[14] N. Scheinowitz, *Development Of A Superconducting Memory Device based on Magnetic Spin Texture*, Master's thesis, Leiden University.

[15] L. Yue and S.-H. Liou, *Magnetic Force Microscopy Studies of Magnetic Features and Nanostructures*, in *Scanning Probe Microscopy in Nanoscience and Nanotechnology 2*, edited by B. Bhushan, NanoScience and Technology, pages 287–319, Springer, Berlin, Heidelberg, 2011.

[16] *NanoWizard3 User Manual*.

[17] M. Vaňatka, M. Urbánek, R. Jíra, L. Flajšman, M. Dhankhar, M.-Y. Im, J. Michalička, V. Uhlíř, and T. Šikola, *Magnetic vortex nucleation modes in static magnetic fields*, AIP Advances **7**, 105103 (2017).

Appendix A

Simulated magnetic patterns of the whole CrO_2 bars

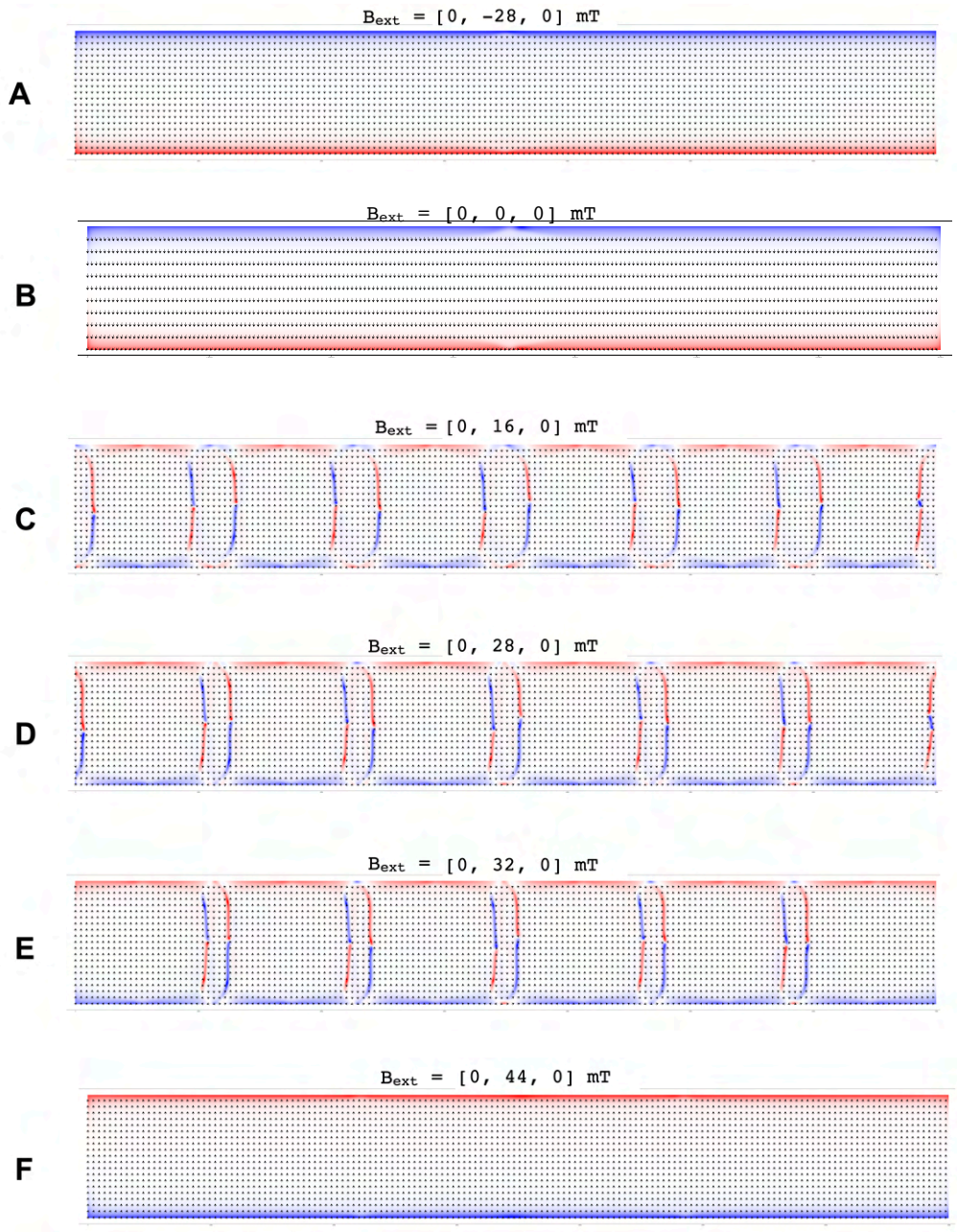

Figure A.1: *Magnetic pattern of the 7 µm x 1 µm x 50 nm CrO_2 bar during the field sweep in the y-direction. The in-plane magnitude is represented by black vectors (a dot representing no magnitude in the x-y plane) and out-of-plane components are represented by the color scale. The length of the bar is represented in nm.*

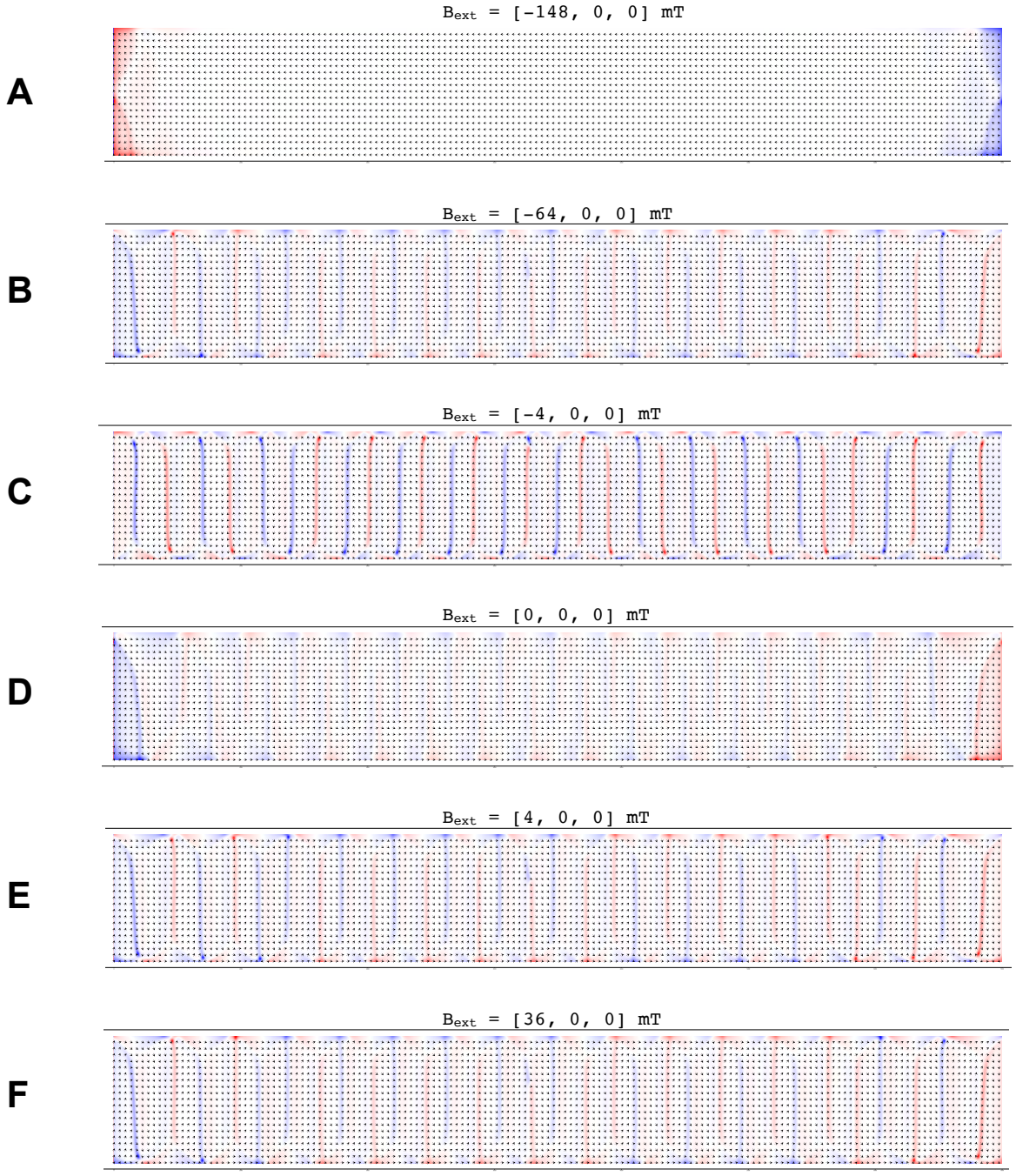

Figure A.2: *Magnetic pattern of the 7 μm x 1 μm x 50 nm CrO_2 bar during the field sweep in the x-direction. The in-plane magnitude is represented by black vectors (a dot representing no magnitude in the x-y plane) and out-of-plane components are represented by the color scale. The length of the bar is represented in nm.*

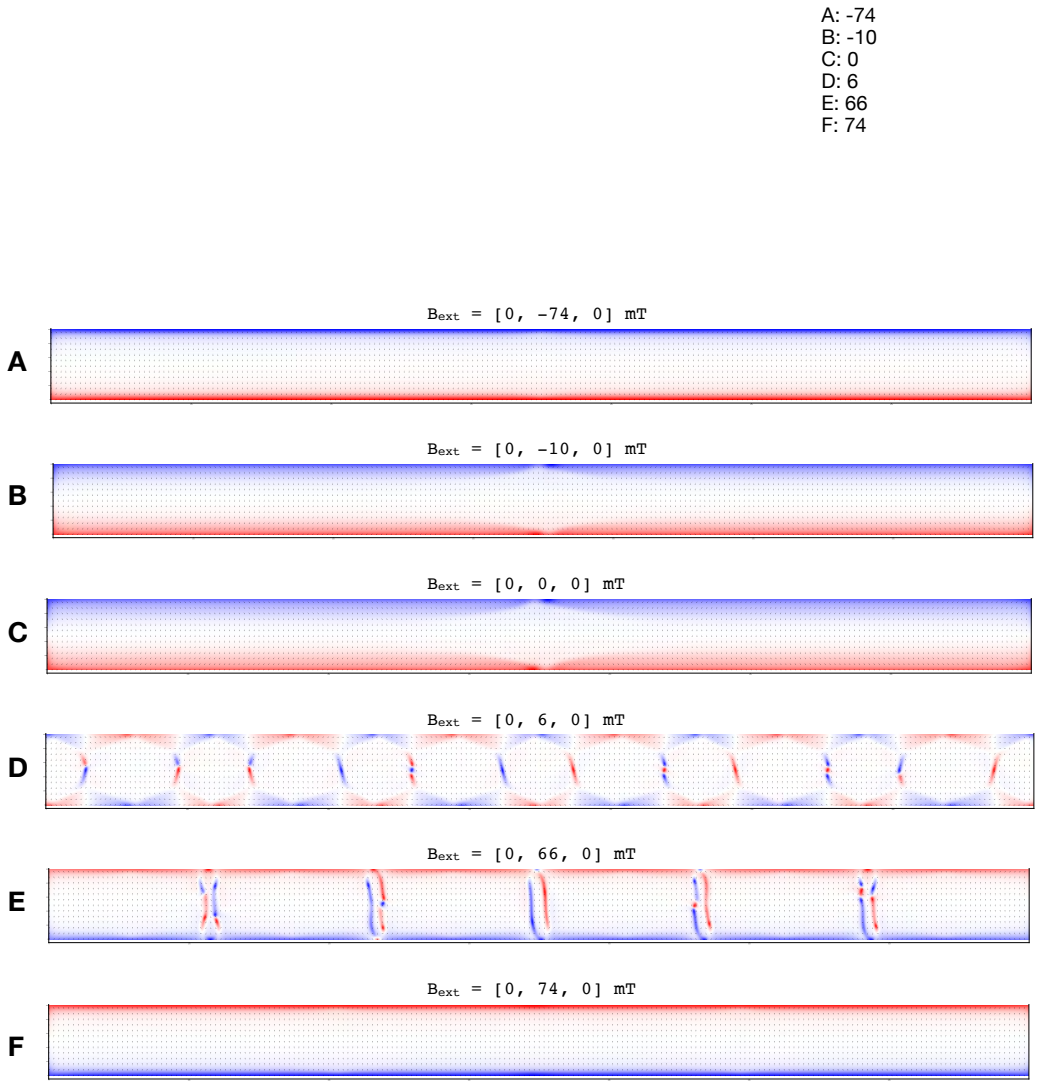

Figure A.3: *Magnetic pattern of the 7 µm x 500 nm x 100 nm CrO_2 bar during the field sweep in the y-direction. The in-plane magnitude is represented by black vectors (a dot representing no magnitude in the x-y plane) and out-of-plane components are represented by the color scale. The length of the bar is represented in nm.*

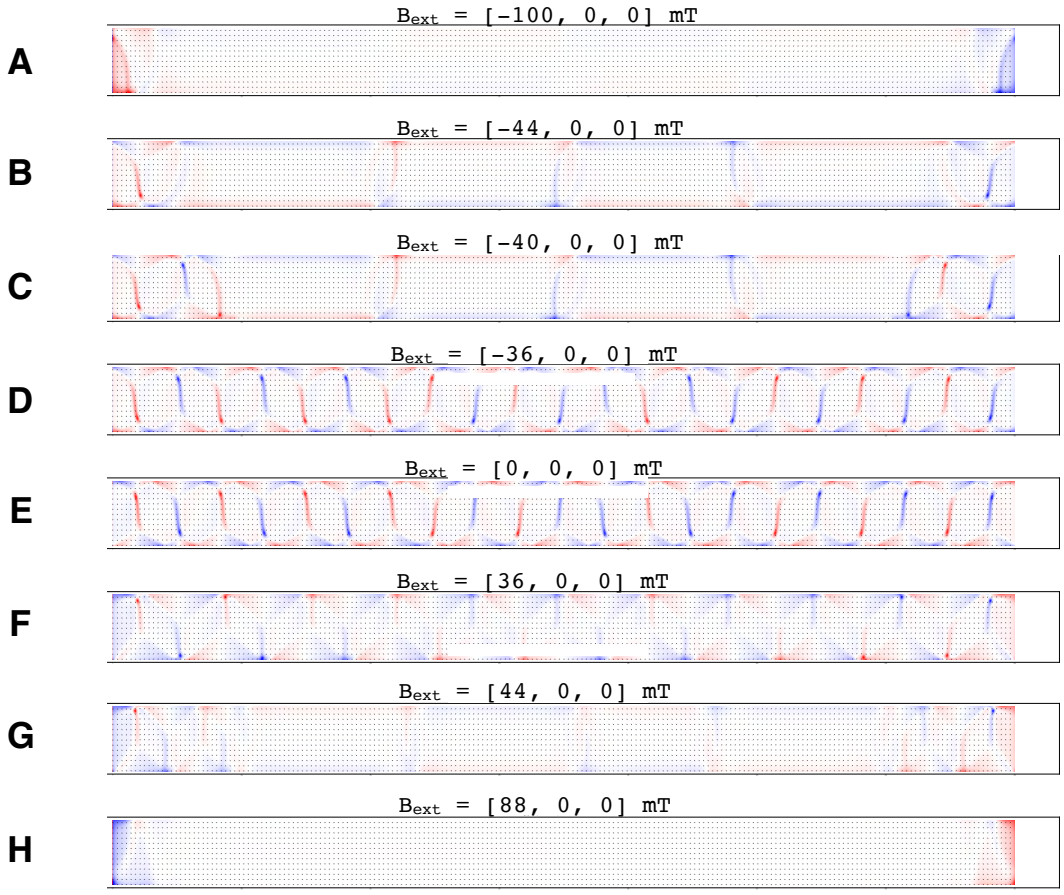

Figure A.4: *Magnetic pattern of the 7 μm x 500 nm x 100 nm CrO_2 bar during the field sweep in the x-direction. The in-plane magnitude is represented by black vectors (a dot representing no magnitude in the x-y plane) and out-of-plane components are represented by the color scale. The length of the bar is represented in nm.*

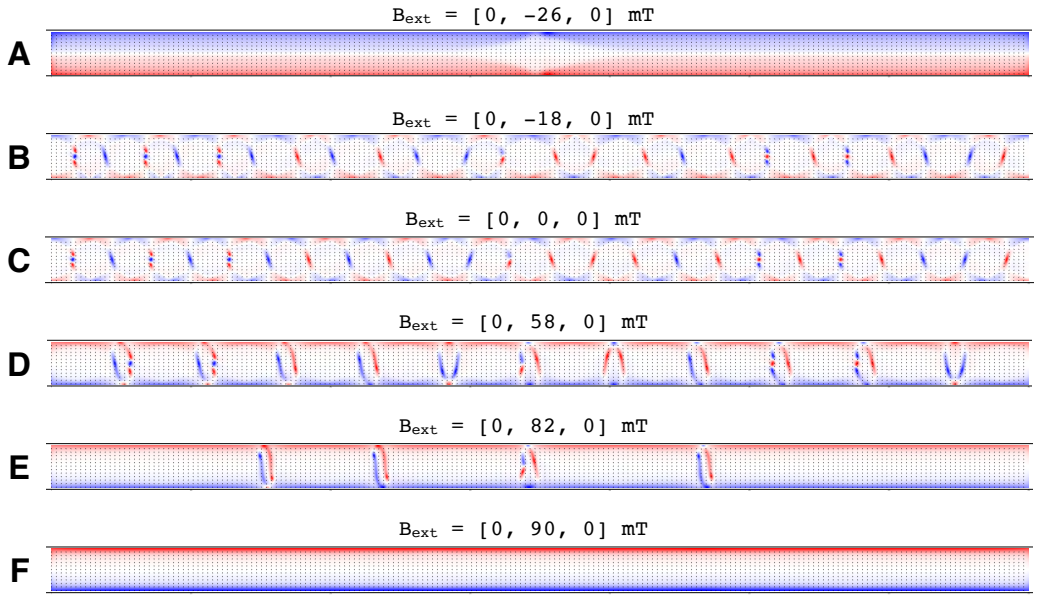

Figure A.5: *Magnetic pattern of the 7 μm x 300 nm x 100 nm* CrO_2 *bar, zoomed in to the part of the bar with the length ranging from 0 μm to 2.5 μm, during the field sweep in the y-direction. The in-plane magnitude is represented by black vectors (a dot representing no magnitude in the x-y plane) and out-of-plane components are represented by the color scale. The length of the bar is represented in nm.*

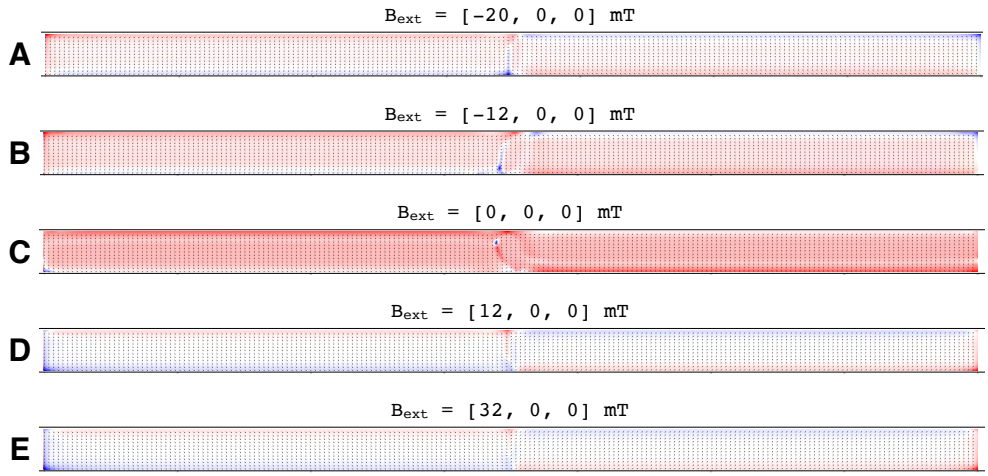

Figure A.6: *Magnetic pattern of the 7 μm x 300 nm x 100 nm CrO_2 bar during the field sweep in the x-direction. The in-plane magnitude is represented by black vectors (a dot representing no magnitude in the x-y plane) and out-of-plane components are represented by the color scale. The length of the bar is represented in nm.*